ELSEVIER

Spectrochimica Acta Part B 53 (1998) 437–462

SPECTROCHIMICA ACTA
PART B

Comprehensive description of a Grimm-type glow discharge source used for optical emission spectrometry: a mathematical simulation

A. Bogaerts[a,*], R. Gijbels[a]

[a]*University of Antwerp, Department of Chemistry, Universiteitsplein 1, B-2610 Wilrijk-Antwerp, Belgium*

Received 6 October 1997; accepted 26 November 1997

Abstract

A three-dimensional modeling network, consisting of different models for describing the behavior of the various species present in a direct current argon glow discharge with copper cathode, has been applied to the Grimm-type glow discharge cell. The modeling results (e.g. the electrical current as a function of pressure and voltage, the potential distribution throughout the discharge, density profiles and energies of the various plasma species, information about collision processes in the plasma and of cathode sputtering) are presented at typical discharge conditions used for glow discharge optical emission spectrometry. The influence of pressure, voltage and current on the calculated results is investigated and a comparison is made with the values obtained in our previous work for typical glow discharge mass spectrometry conditions. The calculation results are compared with experimental data whenever available and in general good agreement is reached, which demonstrates that the models present a realistic picture of the Grimm-type glow discharge. © 1998 Elsevier Science B.V.

Keywords: Modeling; Glow discharge; Grimm source; Optical emission spectrometry

1. Introduction

Glow discharges are used in analytical chemistry as spectroscopic sources, mainly for mass spectrometry and optical emission spectrometry. To improve the analytical results a good insight into the fundamental processes is desirable. We try to obtain this by mathematical modeling, i.e. simulation of the behavior of the most important plasma species and calculation of the characteristic plasma quantities. In the last few years we have developed a comprehensive modeling network for an argon direct current glow discharge used as ion source for mass spectrometry [1–14]. The various calculation results were presented for the typical operating conditions of glow discharge mass spectrometry (GDMS), i.e. about 600–1400 V discharge voltage, 50–100 Pa gas pressure and a few mA electrical current. Glow discharge optical emission spectrometry (GD–OES) works typically at higher gas pressures and electrical currents (i.e. generally a few hundred Pa and 10–100 mA). In the present work we have applied our modeling network to typical GD–OES discharge conditions in order to obtain a better knowledge of the typical values for the characteristic plasma quantities and to compare them with typical GDMS results.

Most GD–OES analyses are performed with the Grimm-type source, first introduced by Grimm in 1968 [15]. One characteristic for this cell type is that the anode (which forms the cell body) approaches the cathode very closely (at a distance shorter than the

* Corresponding author. Tel: 0032 3820 2364; Fax: 0032 3820 2376; e-mail: bogaerts@uia.ua.ac.be.

PII S0584-8547(97)00148-1

length of the cathode dark space) so that no glow discharge plasma is created at this position and the plasma is restricted to a well-defined part of the sample surface. It is therefore called an 'obstructed discharge'. The Grimm source forms the basic design of all commercial optical emission instruments, and a large number of GD–OES analyses (especially depth-profiling) with this source can be found in the literature (e.g. [16–23]). Besides GD–OES applications the Grimm source has also been used in combination with mass spectrometry by Jakubowski and coworkers [24–27]. Moreover, a variety of plasma diagnostic studies have been performed on the Grimm source (e.g. study of the importance of asymmetric charge transfer, atomic absorption experiments to measure number densities of plasma species, Stark spectroscopy to measure the electric field distribution, Langmuir probe measurements and optical emission spectrometry to measure excitation temperatures [28–37]). Finally, a more exotic application of a Grimm glow discharge has recently been reported in which it is used as a new electron and soft X-ray source [38]. To the authors' knowledge, mathematical modeling of a Grimm source has not yet been carried out before and we hope therefore that the present paper will be interesting for the many users of Grimm-type GD–OES.

2. Description of the model

The various models that we have developed for the argon glow discharge are explained in detail in [1–14]. In this paper only a short description will be given. The species assumed to be present in the plasma include electrons, argon gas atoms at rest and uniformly distributed throughout the discharge, argon ions, fast argon atoms, argon atoms excited to various levels, and atoms and ions of the cathode material. These species are described with Monte Carlo or with fluid models.

In the Monte Carlo simulations the trajectory of the particles is described with Newton's laws and the probability of collisions, the nature of a collision, the new energy and direction after collisions are determined by random numbers. By following in this statistical way a large number of particles, the glow discharge can be simulated. This method is very accurate because it deals with the particles on the lowest microscopic level, but it requires detailed knowledge of cross sections as a function of energy and also considerable calculation time for slow-moving particles. The fluid models that we use, on the other hand, are based on continuity equations (conservation of number density with balance equations taking into account a variety of production and loss processes) and on transport equations (describing diffusion and also migration in the electric field for charged particles). This model is actually based on thermal equilibrium with the electric field. Energetic species (like electrons) are not in such equilibrium and cannot be described accurately enough with this model. However, this approach is valid for slow particles for which it is generally faster and more efficient than the Monte Carlo simulations. Hence, both of these modeling approaches have their advantages and disadvantages. Therefore, in our comprehensive modeling network we use a combination of Monte Carlo and fluid models for the various plasma species. The Monte Carlo simulations are developed in three dimensions; the fluid models are two-dimensional, because the three dimensions can generally be reduced to two dimensions due to the cylindrical symmetry of the glow discharge cells being considered.

A short description of the different models for the various species (e.g. the processes taken into account) is given here.

(a) Monte Carlo model for electrons [1–3]: the electrons will generally gain more energy from the electric field than they lose by collisions. Hence, they are not in equilibrium with the electric field and must preferably be described with a Monte Carlo model. The collision processes incorporated in this model are elastic collisions with argon gas atoms, electron–electron Coulomb collisions, electron impact ionization from the ground state and from various (64) excited levels, excitation and de-excitation between all these levels and electron–ion recombination to all levels.

(b) Fluid model for argon ions and slow electrons [2,3]: the electrons are actually split up into two electron groups; fast and slow. Electrons are in general called 'fast' when they possess sufficient energy for producing inelastic collisions. Since it is computationally-intensive to follow the slow electrons with a Monte Carlo model these species are

generally described with a fluid model. Only when detailed information is required about the various (de-)excitation rates between the excited levels (i.e. for calculating the population densities of these levels) are the slow electrons simulated with the Monte Carlo model. For all other purposes we treat them with a fluid model together with the argon ions. The continuity and transport equations of electrons and argon ions are coupled to the Poisson equation to obtain a self-consistent electric field distribution.

(c) Monte Carlo model for the argon ions and fast argon atoms in the cathode dark space (CDS) [1,3,4]: the argon ions are not in equilibrium with the high electric field in the region adjacent to the cathode (called 'cathode dark space'). Therefore, they are described in this region with a Monte Carlo model, together with the fast argon atoms which are created from the argon ions by symmetric charge transfer and elastic scattering collisions. Collision processes taken into account in this model are elastic scattering collisions for both ions and atoms, symmetric charge transfer for ions (which is actually also a kind of elastic collision because there is no change in kinetic energy of the colliding particles), ion and atom impact ionization, excitation and de-excitation for all levels and electron–ion three-body recombination to all levels with the third particle being an argon ion or fast argon atom.

(d) Fluid model for the argon atoms excited to various levels [5,8,9]: the behavior of the argon atoms in various excited levels including the metastable levels (i.e. so-called metastable argon atoms) is described with a set of coupled balance equations (one equation for each level) consisting of various populating and depopulating processes; 65 argon levels are considered. The processes taken into account are electron, argon ion, fast and thermal argon atom impact ionization, excitation and de-excitation for all levels, radiative decay between all levels, radiative electron–ion recombination and three-body electron–ion recombination where the third body is an electron, argon ion, fast or thermal argon atom. Because of the large number of collisional and radiative (de)populating processes, this kind of model is commonly called 'collisional–radiative model'. In [9] this collisional–radiative model has been developed in one dimension. For the present purpose, the model was extended to the three-dimensional geometry (in cylindrical symmetry) of the Grimm source.

(e) Monte Carlo model for the sputtered atoms [6]: when the atoms are sputtered away from the cathode they have typical energies of a few electronvolts. They lose these energies almost immediately by elastic collisions with argon gas atoms until they are thermalized. This thermalization process is simulated with a Monte Carlo model.

(f) Fluid model for the sputtered atoms and ions [7,8]: when the sputtered atoms are thermalized their further transport is diffusion-dominated; they can diffuse further into the plasma or back towards the cathode, leading to redeposition. They can also become ionized due to Penning ionization by argon metastable atoms, asymmetric charge transfer with argon ions or due to electron impact ionization, creating ions of the cathode material. The diffusion of sputtered atoms, their ionization and the transport of the corresponding ions (by diffusion and by migration in the electric field) are described with coupled differential equations in a fluid model.

(g) Monte Carlo model for the ions of the cathode material [7,8]: similar to the argon ions, the ions of the cathode material are not in equilibrium with the strong electric field in the CDS and they are therefore also handled with a Monte Carlo model in this region. Only elastic collisions with argon atoms are incorporated as collision processes; other collisions with argon atoms have clearly lower cross sections and collisions with sputtered atoms are also of minor importance due to their lower density in the plasma. All of these different models are coupled to each other due to the interaction processes between the plasma species, and they are solved iteratively until final convergence is reached to obtain an overall picture of the glow discharge.

3. Results and discussion

The results will be presented for an argon glow discharge with pure copper cathode. The cell geometry corresponds to the Grimm source. Fig. 1 shows a schematic picture of this cell with the typical dimensions used in the model. It is assumed, however, that the cell is in a closed configuration without gas inlet or pumping canal. This assumption is probably justified

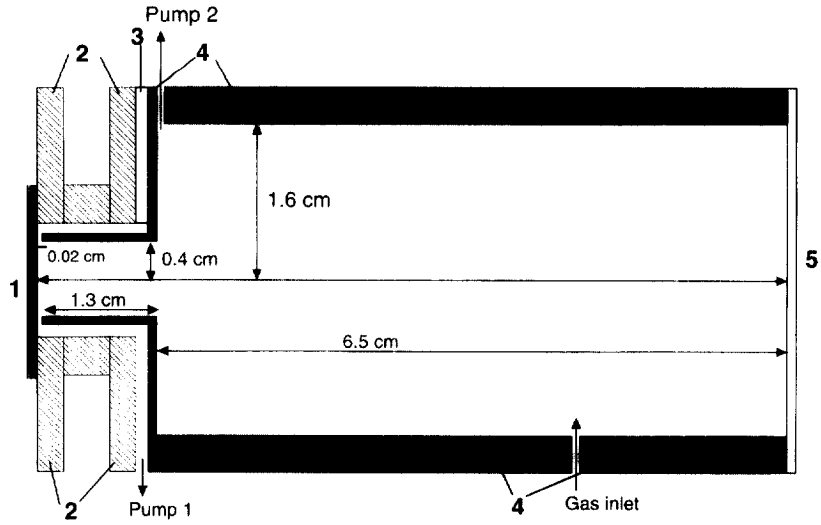

Fig. 1. Schematic representation of the Grimm source geometry, used in the modeling work. (1) Sample, (2) cathode, (3) insulator, (4) anode cell body, (5) quartz window.

since the anode body approaches the cathode so closely here that no glow discharge can be created. Hence the model is restricted to the volume where the glow discharge plasma is really present.

The results are computed for typical discharge conditions used in GD–OES. When pressure, voltage and gas temperature are given the electrical current follows self-consistently as a calculation result of the models, i.e. as the sum of the microscopic fluxes of the charged plasma species. Since the electrical current is a macroscopic quantity which can be measured rather easily, it can be useful for comparison with experimental data as a validation criterion for the models. Fig. 2 presents some calculated current–voltage–pressure characteristics. The current rises clearly with increasing pressure and voltage, which is in correspondence with experimental data. Exact quantitative agreement with experiment, however, cannot yet be expected. Indeed, there are some inherent uncertainties in the cross sections used as input for

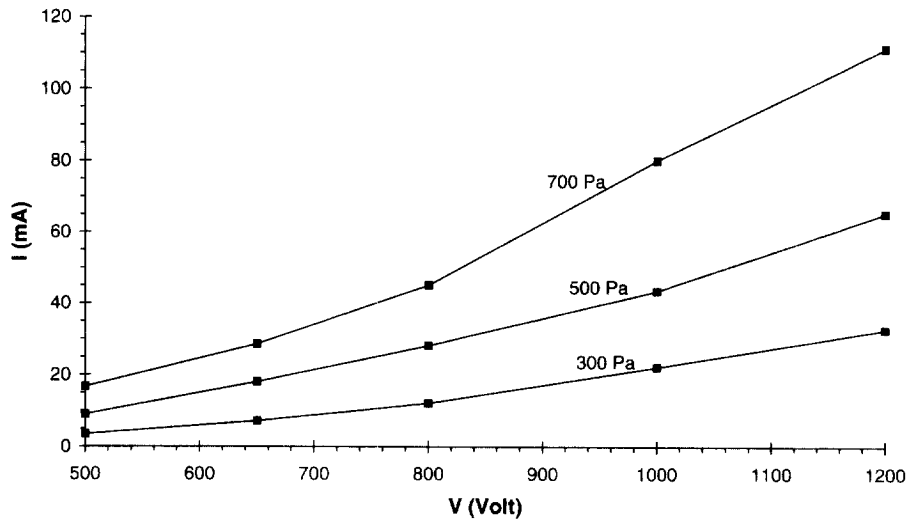

Fig. 2. Calculated electrical currents as a function of voltage at three pressures.

the various collision processes, and since the electrical current is the final result from all calculations, possible errors in the input data will manifest themselves as larger errors in the final results (snowball-effect) and the absolute value of the final electrical current will therefore also be subject to considerable uncertainties. Moreover, the exact gas temperature in the plasma is unknown. From [28] it could be deduced that the gas temperature increases generally with rising current at constant voltage (and hence with rising pressure). Therefore, we assumed a gas temperature of 600 K at 300 Pa, 800 K at 500 Pa and 1000 K at 700 Pa. This is in reasonable agreement with the values reported in [28] for a Grimm-type of discharge, at least for the more moderate discharge conditions (e.g. 800 V, 40 mA); at higher operating conditions (e.g. 800 V, 60 or 80 mA) the measured gas temperatures seem to be even higher than 1000 K. In spite of the uncertainties in the gas temperature and in the cross sections used in the model the calculated currents have the correct order of magnitude. Hence, this is a validation of the reliability of our models and it indicates that the other calculated results will also present a realistic picture of the glow discharge.

The current–voltage–pressure characteristics obtained for GD–OES are generally higher than the corresponding values for GDMS (i.e. more or less the same voltage range, but lower pressures (ca. 100 Pa) and hence lower currents (a few mA)). Therefore, the characteristic plasma quantities will also be clearly higher than the values computed in our earlier papers for GDMS conditions. In the following, the various calculation results will be presented for the typical GD–OES conditions of 500 Pa, 800 V, 28 mA, and the effect of pressure, voltage and current will be discussed.

3.1. Electrical characteristics: potential and electric field distributions

As mentioned before, the potential and electric field distributions follow self-consistently from the modeling network, i.e. the electric fields used in the Monte Carlo models to simulate the behavior of the electrons and ions are calculated in their turn from the electron and ion number densities with the Poisson equation in one of the fluid models.

The two-dimensional potential distribution throughout the discharge, at 500 Pa, 800 V and 28 mA, is illustrated in Fig. 3 (cross section of the cylindrically symmetrical cell). The cathode is at z = 0 cm; the anode cell body forms the other borders of the figure, as well as the grey rectangles from z = 0.02–1.3 cm. The potential is − 800 V at the cathode and increases very rapidly until it reaches zero at about 0.07 cm from the cathode. This position where the potential crosses the zero-line is defined as the interface between cathode dark space (CDS) and negative glow (NG). Hence the CDS is only

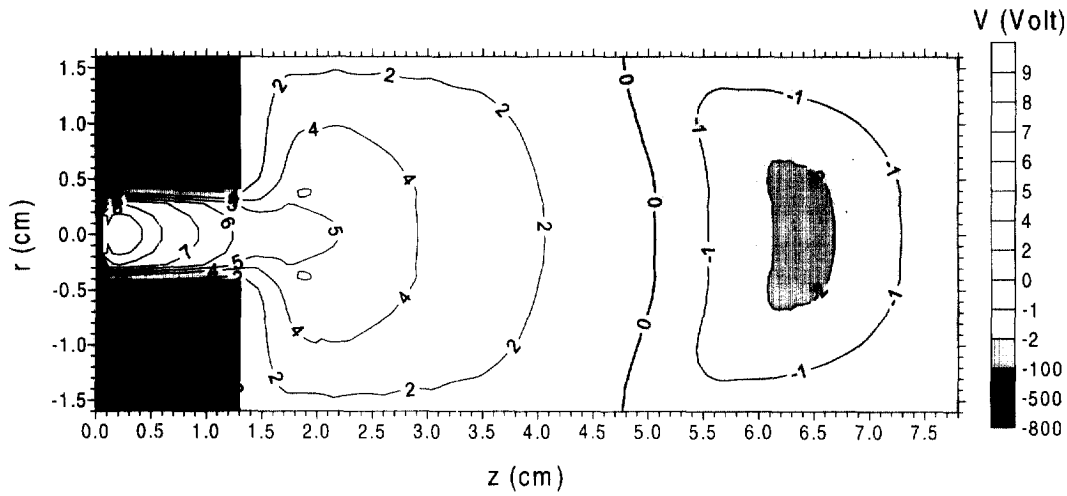

Fig. 3. Calculated two-dimensional potential distribution throughout the discharge cell (cylindrical symmetry) at 500 Pa, 800 V and 28 mA.

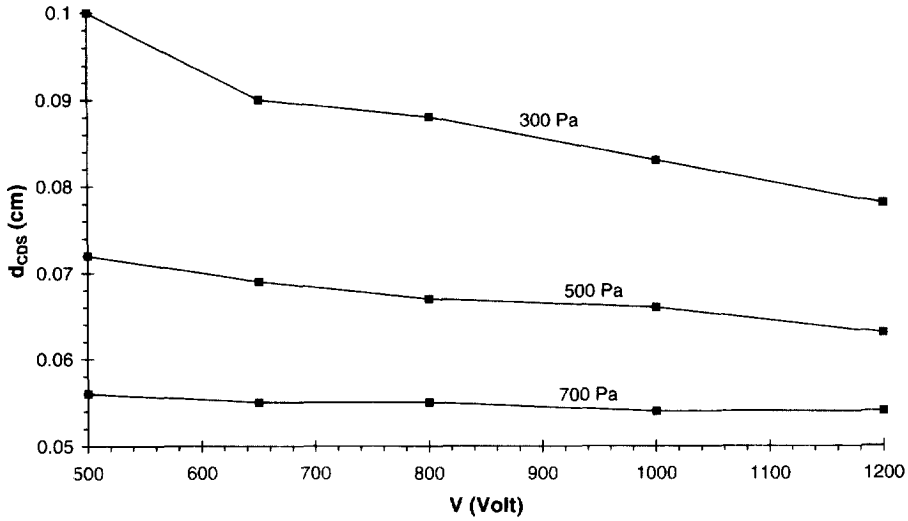

Fig. 4. Calculated lengths of the cathode dark space (d_{CDS}) as a function of voltage at three pressures.

about 0.07 cm long at these discharge conditions. This value is clearly lower than the typical values calculated for GDMS conditions (i.e. about 0.1–0.3 cm [3,4,13]). Indeed, the length of the CDS decreases clearly with increasing pressure, as can also be observed in Fig. 4. At 300 Pa typical values of 0.08–0.1 cm were calculated, at 500 Pa this value was about 0.07 cm, and at 700 Pa lengths of 0.05–0.06 cm were obtained. The voltage does not seem to have a large effect on the calculated CDS lengths; the latter increase only slightly with decreasing voltages. Since the anode body approaches the cathode as close as 0.02 cm in the Grimm source, the anode–cathode distance is kept lower than the length of the CDS so that no glow discharge can be created at this place, and hence the Grimm-type discharge is indeed 'obstructed'.

After crossing the zero-line the potential increases a little to reach a slightly positive value in the NG (Fig. 3)—the maximum is located between 0.1 and 0.4 cm and is about 9 V; this is called the 'plasma potential'. This value of about 9 V seems to be nearly independent of the discharge conditions; it increases only slightly (less than 1 V) with voltage. However, this value depends strongly on the cell dimensions, as was demonstrated in [13].

After this maximum the potential decreases again. The cells that we have modeled before were typically 1–2 cm long; in those cells the calculated potential decreased after the maximum (plasma potential) to reach zero at the anode walls, so that only CDS, NG and a small anode dark space (ADS) were present [3,13,14]. The Grimm source, however, is typically much longer and we see the appearance of a Faraday dark space (FDS) and maybe also a short positive column (PC). Indeed, as follows from Fig. 3, the potential decreases after the maximum in the NG and it crosses zero at about 5 cm from the cathode. After a local minimum of about − 2 V at 6–6.5 cm it increases again to reach zero at the anode backplate. This potential increase at the end of the cell (in the FDS and PC) is required to draw the electrons out of the plasma. Indeed, as the cell becomes longer, more and more electrons are thermalized and cannot reach the anode cell walls anymore. The potential increase in front of the anode attracts the electrons and guarantees that sufficient electrical current arrives at the anode.

The electric field distribution follows immediately from the potential distribution by the first derivative with respect to distance and is therefore not shown here. The axial electric field is extremely negative at the cathode since a large potential difference (ca. 500–1200 V) has to drop over a very short distance (less than 0.1 cm). Generally, the axial electric field at the cathode increases with rising voltage (since a larger potential difference has to be bridged) and also with rising pressure (due to the

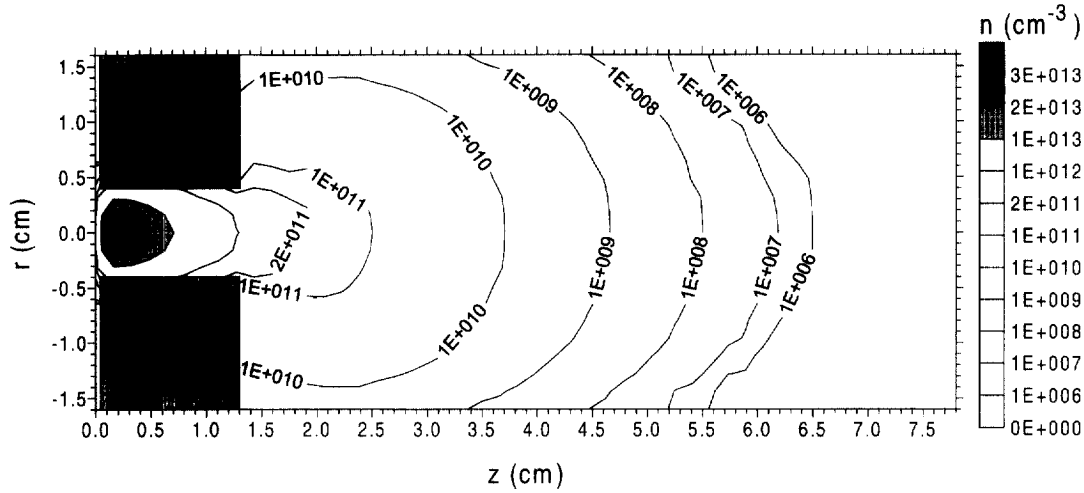

Fig. 5. Calculated two-dimensional density profile of the argon ions throughout the discharge cell at 500 Pa, 800 V and 28 mA.

shorter CDS length, see above). For the discharge conditions that we have investigated this value ranges from about -11 kV cm^{-1} at 500 V, 300 Pa and 3.5 mA to about -76 kV cm^{-1} at 1200 V, 700 Pa and 110 mA.

Away from the cathode the axial electric field rises rapidly and reaches zero at a few mm from the cathode: it is slightly positive in the rest of the plasma (a few V cm^{-1}); indeed, it is generally accepted that the NG is nearly field-free. At about 6 cm from the cathode it becomes slightly negative (i.e. where the small potential increase takes place) as is required to attract a sufficiently large electron current towards the anode (see above). In general, the axial electric field is always of the order of only a few V cm^{-1}, except in the CDS close to the cathode. The radial electric field, on the other hand, was found to be a little bit higher, especially in the first part of the discharge ($z <$ 1.3 cm) where the potential has to fall off towards the walls over a rather short distance. In this region the radial electric field reaches values in the order of 100 V cm^{-1} at the cell walls.

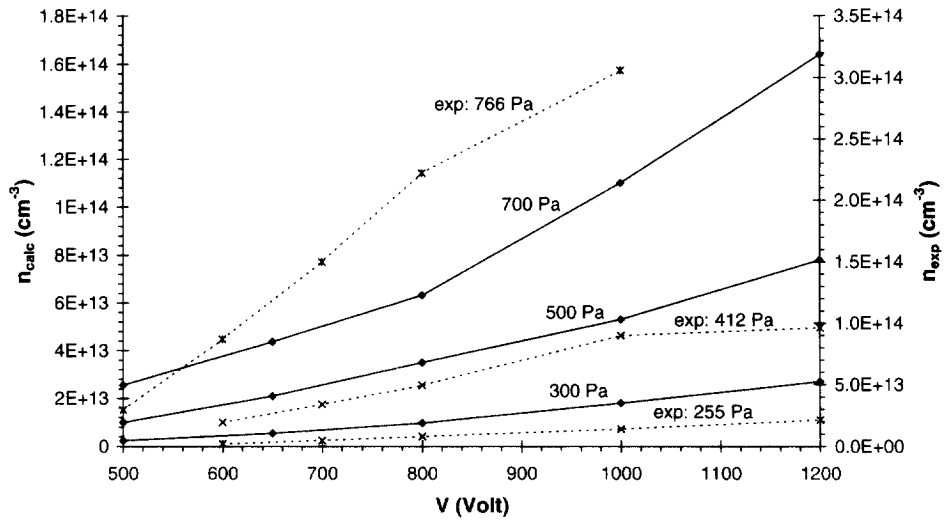

Fig. 6. Calculated densities of the argon ions and slow electrons at the maximum of their profiles as a function of voltage at three pressures (solid lines, left axis), and experimental slow electron densities, measured with Langmuir probe measurements (dashed lines, right axis).

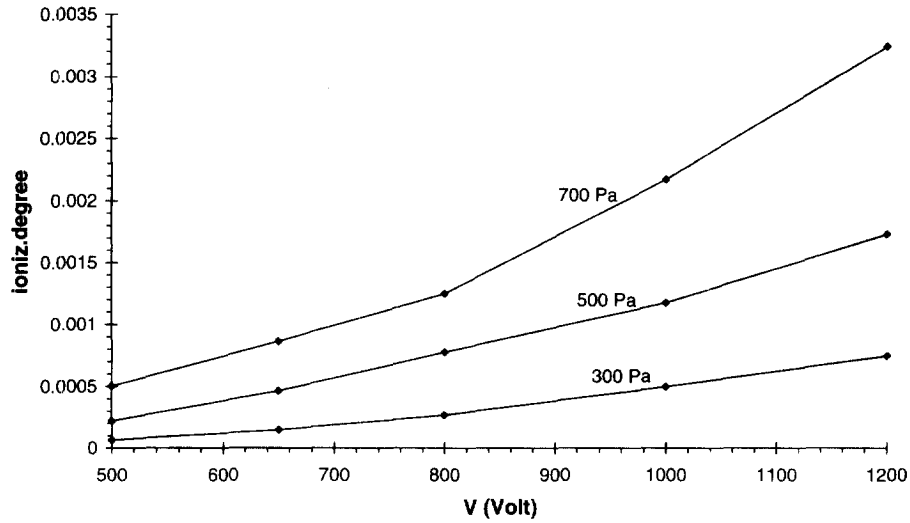

Fig. 7. Calculated ionization degrees of argon as a function of voltage at three pressures.

3.2. Number densities of plasma species

3.2.1. Argon ions and slow electrons

Fig. 5 illustrates the argon ion number density at 800 V, 500 Pa and 28 mA. The density is low and rather constant in the CDS and reaches a maximum of about 3×10^{13} cm^{-3} at 0.2 cm from the cathode. This is considerably higher than the values calculated for typical GDMS conditions (i.e. 10^{11}–10^{12} cm^{-3} [2,3,13,14]). The density gradually decreases further in the discharge cell and behind about 1.3 cm, in the extended part of the cell, it drops over more than six orders of magnitude. The slow electron number density is characterized by more or less the same profile. It is zero in the CDS, yielding a net positive space charge and hence a potential increase in this region. In the NG the argon ion and slow electron densities are nearly equal to each other, resulting in charge neutrality. In the FDS, however, the slow electron density becomes slightly higher than the argon ion density, which gives rise to the small negative axial electric field at the end of the cell.

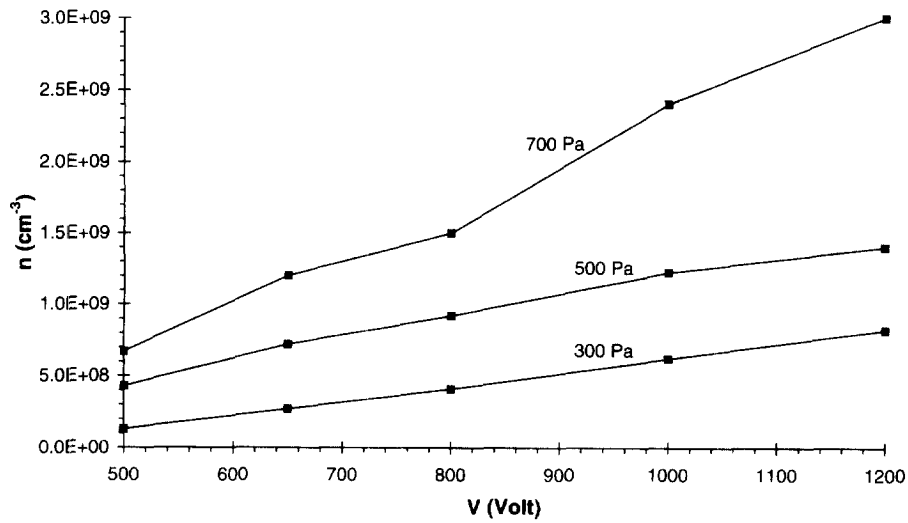

Fig. 8. Calculated densities of the fast electrons at the maximum of their profiles, as a function of voltage at three pressures.

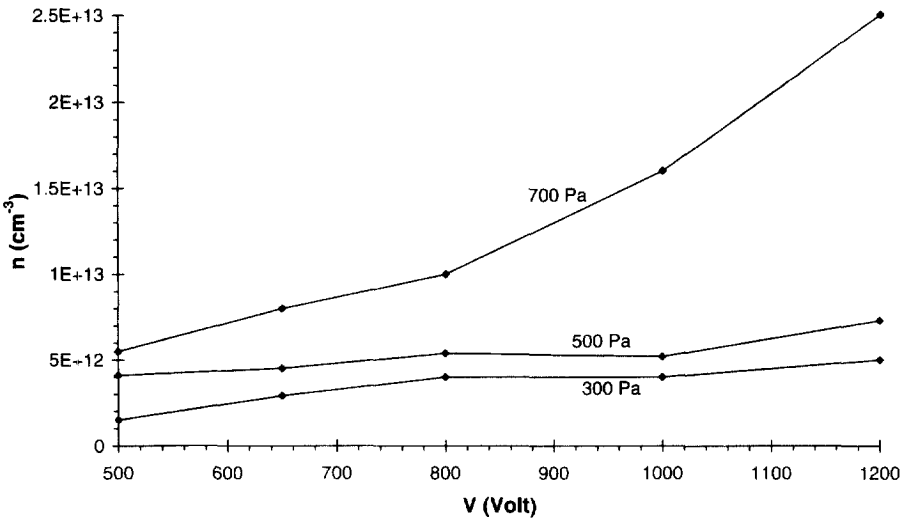

Fig. 9. Calculated densities of the fast argon atoms at the maximum of their profiles, as a function of voltage at three pressures.

The argon ion and slow electron number densities increase clearly with rising voltage and pressure, as appears from Fig. 6, where the densities at the maximum of the profiles are plotted against voltage for three different pressures. The increase is similar to the variation of current as a function of pressure and voltage (see above, Fig. 2). This is as expected since the argon ion and slow electron number densities are in close correlation with the fluxes of these species and the latter determine the electrical current. Therefore, the current does indeed behave as a function of pressure and voltage in the same manner as the argon ion and slow electron densities.

We have also determined slow electron number densities experimentally in a Grimm source by Langmuir probe measurements [35] and the results for an argon discharge with copper cathode, measured at about 7 mm from the cathode, are presented in Fig. 6 as well (dashed lines, right axis). The pressures are not exactly equal, but they are in the same order of magnitude. In spite of the fact that the experiments were performed in a Grimm cell, which is normally used for GDMS analyses [24–27], with a slightly different geometry from the one used for the modeling work, the experimental and calculation results are in satisfactory agreement: the difference is only a factor of about two, which is well below the uncertainties expected for both the modeling and Langmuir probe results.

When comparing the argon ion number densities with the densities of argon gas atoms, the ionization degree of argon can be deduced. The argon gas atom density is determined from the gas pressure and temperature with the ideal gas law ($n = kT/p$). This yields the following argon atom densities: $n_{Ar} = 3.6 \times 10^{16} cm^{-3}$ at 300 Pa, 600 K, $n_{Ar} = 4.5 \times 10^{16} cm^{-3}$ at 500 Pa, 800 K and $n_{Ar} = 5.1 \times 10^{16} cm^{-3}$ at 700 Pa, 1000 K. The ionization degrees calculated from the argon ion and atom densities are plotted in Fig. 7 as a function of voltage at the three pressures investigated. The values clearly increase with voltage and pressure. They range from 7×10^{-5} at low voltage and pressure to about 3×10^{-3} at the highest voltage and pressure investigated. This is somewhat higher than the values determined for typical GDMS conditions (i.e. in the order of 10^{-5} [39]). However, the calculated values are still lower than 1% at all discharge conditions under study, hence it can be concluded that the argon glow discharge is only a weakly ionized plasma.

3.2.2. Fast electrons

The fast electron number density reaches a maximum at about 1 mm from the cathode (i.e. in the beginning of the NG) and it decreases further in the cell. Fig. 8 shows the density at the maximum of the profile as a function of voltage at the three different pressures. It has typical values of 10^8–$3 \times 10^9 cm^{-3}$

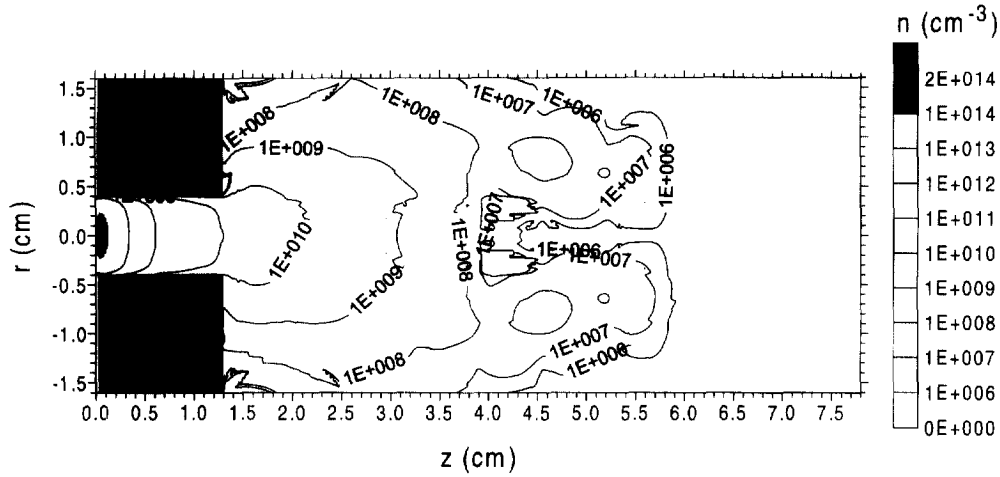

Fig. 10. Calculated two-dimensional density profile of the sputtered copper atoms throughout the discharge cell at 500 Pa, 800 V and 28 mA.

and also increases with voltage and pressure. These densities are almost five orders of magnitude lower than the corresponding argon ion and slow electron number densities (see Fig. 6). Hence the fast electrons do not play any role in determining the space charge. They are, however, extremely important in the glow discharge plasma because they give rise to ionization collisions, which is necessary to maintain the electrical current throughout the discharge.

3.2.3. *Fast argon atoms*

The term 'fast' argon atoms is used for those atoms with energies above thermal energy (i.e. ca. 0.1 eV). These species are only present in the CDS, because they are formed from the argon ions in this region by elastic scattering and charge transfer collisions. In the NG the argon atoms are generally thermalized. The fast argon atom number density at the maximum of its profile is presented in Fig. 9 as a function of voltage and pressure. It increases with pressure and voltage

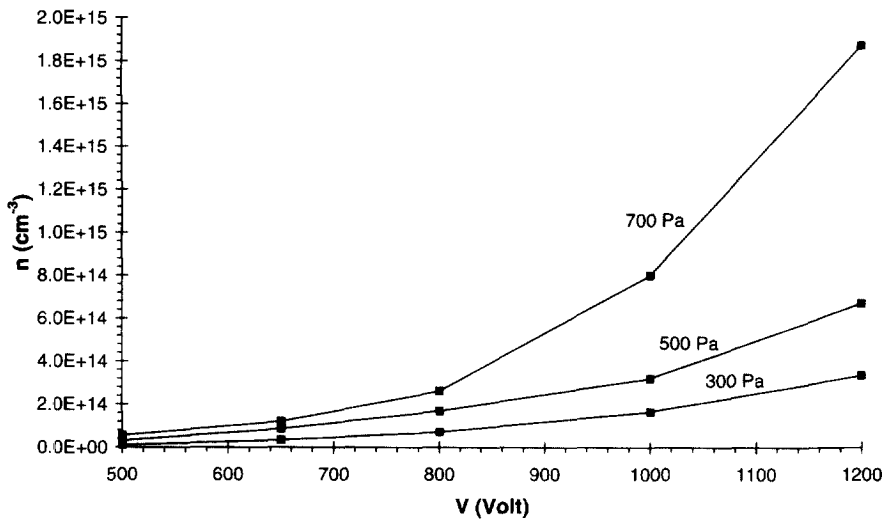

Fig. 11. Calculated densities of the sputtered copper atoms at the maximum of their profiles, as a function of voltage at three pressures.

and ranges from about 1.5×10^{12} cm^{-3} to about 2.5×10^{13} cm^{-3}. These values are 3–4 orders of magnitude lower than the overall argon atom density (see above), so it can be concluded that in general the argon gas is thermalized.

In spite of their low number density the fast argon atoms play a significant role in the glow discharge, for sputtering at the cathode and for ionization and excitation of argon atoms, as will be shown later.

3.2.4. Sputtered copper atoms

Fig. 10 illustrates the two-dimensional number density profile of sputtered copper atoms at 500 Pa, 800 V and 28 mA. The density reaches a maximum adjacent to the cathode (at about 0.05 cm) and gradually decreases further in the discharge cell. The total density of copper atoms is the sum of thermalized and non-thermalized atoms. The density of the latter is, however, many orders of magnitude lower and hence negligible compared to the thermalized atom density. Indeed, the majority of sputtered copper atoms are thermalized already at less than 1 mm from the cathode at the high pressures used for GD–OES.

The copper atom density at the maximum of the profile is plotted against voltage at three pressures in Fig. 11. It varies from 1×10^{13} cm^{-3} at low voltages and pressures to about 2×10^{15} cm^{-3} at high voltages and pressures. This corresponds to a fraction of about 3×10^{-4} to 4×10^{-2} of the argon gas atom density. Hence, the copper atoms have still a more or less negligible density at the low voltages and pressures, but this is not true anymore at the high voltages and pressures where its density amounts to a few percent of the argon atom density. Therefore, the sputtered copper atoms are more abundant in the discharge compared to GDMS conditions where typical density values of 10^{11}–10^{13} cm^{-3} (i.e. 3–5 orders of magnitude lower than the argon atom density) were encountered (e.g. [7,8,13,14,39]).

Ferreira and coworkers have measured sputtered copper atom densities in a Grimm source by atomic absorption spectrometry (AAS) [29]. They obtained values of about 3×10^{13} cm^{-3} at the maximum of the profile (i.e. also at 0.25–0.5 mm from the cathode) for the discharge conditions of 800 V, 40 mA and 1000 V, 40 mA. These voltage–current values correspond more or less to our pressures of 700 and 500 Pa, respectively, at which we computed copper atom densities at the maximum of the profiles of about 3×10^{14} cm^{-3} (see Fig. 11). This value is an order of magnitude higher than the experimental results, which suggests that either the model calculates too high densities or that the experimental work yielded too low values; most probably it is a combination of both effects. In [40] we have measured sputtered tantalum atom density profiles, both with laser induced fluorescence (LIF) and with a combination of LIF and AAS, and the results have been compared with calculated values for exactly the same geometry and

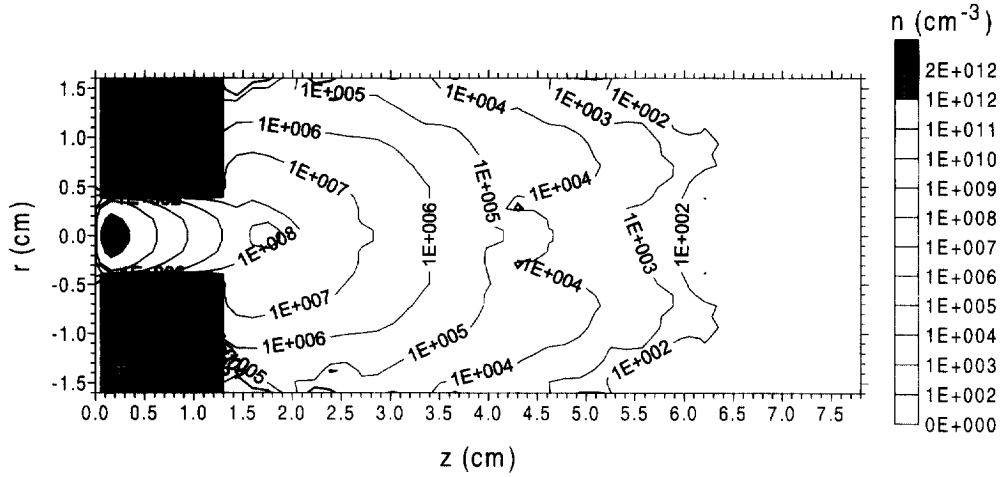

Fig. 12. Calculated two-dimensional density profile of the copper ions throughout the discharge cell at 500 Pa, 800 V and 28 mA.

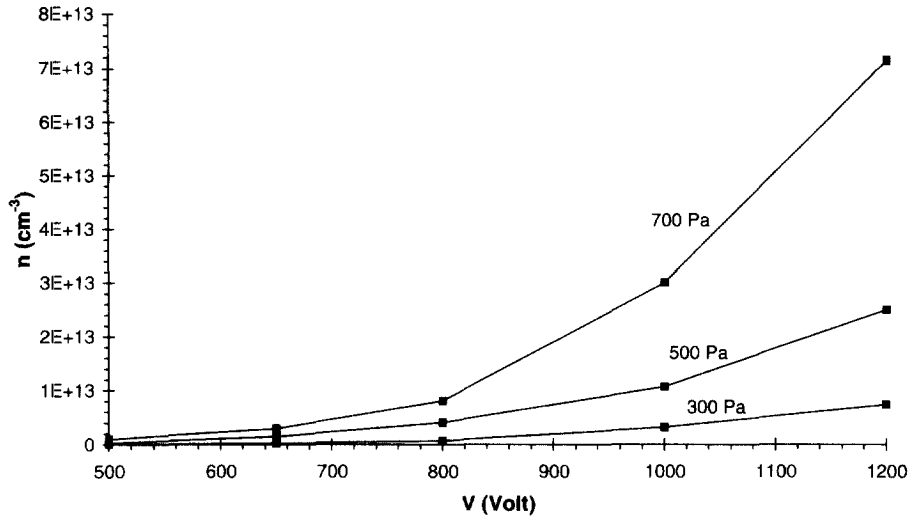

Fig. 13. Calculated densities of the copper ions at the maximum of their profiles, as a function of voltage at three pressures.

discharge conditions. The results of the two experimental methods differed by a factor of about three and the calculated values were found to lie in between them. This illustrated on the one hand that the experimental data can also be subject to errors and on the other hand that the model calculates already realistic values in the correct order of magnitude. After all, we cannot yet expect perfect agreement with experimental data because there are too many parameters subject to uncertainties in the entire model; hence a factor of 10 difference does not appear too bad at all.

Hoffmann et al. measured lateral distributions of the sputtered atoms in a Grimm source (end-on observations) and they obtained a parabolic profile with the maximum at the cell axis if the atoms were distributed homogeneously over the sample surface [21]. This characteristic parabolic profile is also found back in our calculations, as can be deduced from Fig. 10.

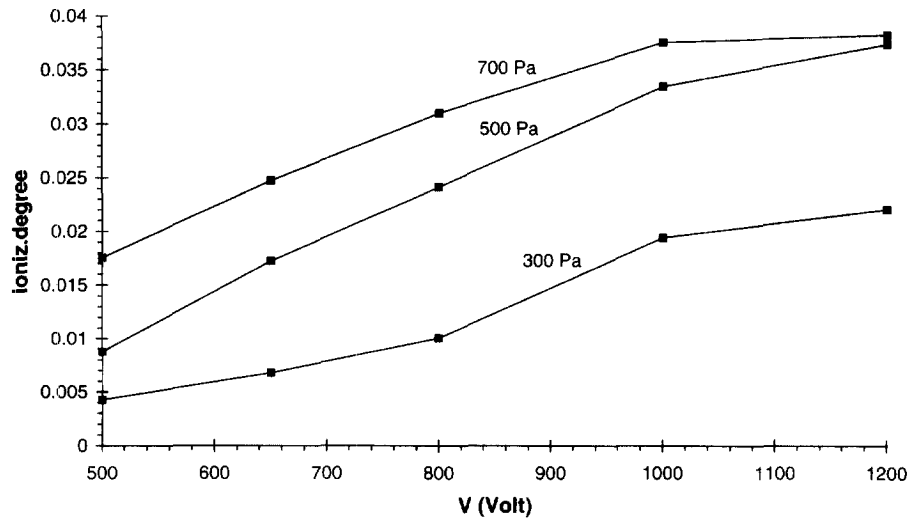

Fig. 14. Calculated ionization degrees of the sputtered copper atoms as a function of voltage at three pressures.

3.2.5. Copper ions

The copper ion number density profile is characterized by a maximum at about 2 mm from the cathode and decreases further in the plasma, as follows from Fig. 12, where the two-dimensional density profile is presented at 500 Pa, 800 K and 28 mA. The density profile is similar to the one calculated for argon ions (see Fig. 5), but the absolute values are lower (i.e. a factor of about 10 at the maximum, but several orders of magnitude further in the discharge).

Fig. 13 presents the copper ion density at the maximum of its profile as a function of voltage and pressure. The density varies from 5×10^{10}cm^{-3} to 7×10^{13}cm^{-3}, rising with both voltage and pressure. Hence, it is always lower than the maximum argon ion density (i.e. 2×10^{12}–1.6×10^{14}cm^{-3}; see Fig. 6), but the difference becomes smaller at high voltages and pressures. Indeed, the ratio of copper ion to argon ion density at the maximum is a few percent at low pressure and voltage and it rises to nearly 50% at the highest pressure and voltage investigated. At typical GDMS conditions the copper ion density ranged from 10^{6}–10^{11}cm^{-3} and the ratio with respect to the argon ion density varied from 10^{-4} to a few percent (e.g. [7,8,39]). Hence, not only the sputtered copper atoms but also the corresponding ions become more significant in the glow discharge at GD–OES compared to GDMS conditions.

From the above comparisons, it also becomes clear that the density ratio of copper ions to argon ions (i.e. a few percent to 50%) is higher than the corresponding ratio of copper to argon atoms (i.e. 0.03–4%). This indicates that the copper atoms are more efficiently ionized than the argon atoms, as will be demonstrated later. The latter conclusion follows also from the calculated ionization degree of copper (i.e. the density ratio of copper ions to copper atoms, computed at their maximum) which rises from 0.4 to 4% with increasing pressures and voltages, as appears from Fig. 14. These values are clearly higher than for GDMS conditions where ionization degrees for copper of typically 0.01–0.4% were computed [8,39]. The copper ionization degrees are also more than one order of magnitude higher than the corresponding values for argon. However, the values do not increase with voltage to the same extent as is the case for argon. Indeed, the argon ion density rises with voltage and the argon atom density remains constant (see above), whereas for copper both the ion and atom densities increase as a function of voltage. Nevertheless, the copper ion density seems to vary more than the atom density so that the ionization degree increases with voltage, which means that the ionization still becomes more efficient at higher voltages.

3.2.6. Argon excited atoms

Fig. 15 presents the two-dimensional population density of the 4s $[3/2]_2$ metastable argon atom level, i.e. the lowest excited level of the argon atom (at 11.55 eV), throughout the discharge at 500 Pa,

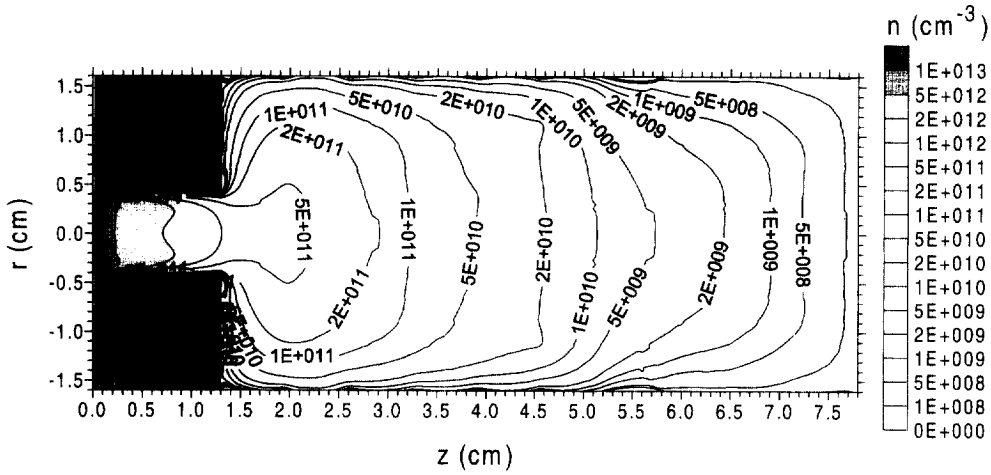

Fig. 15. Calculated two-dimensional density profile of the argon 4s $[3/2]_2$ metastable level throughout the discharge cell at 500 Pa, 800 V and 28 mA.

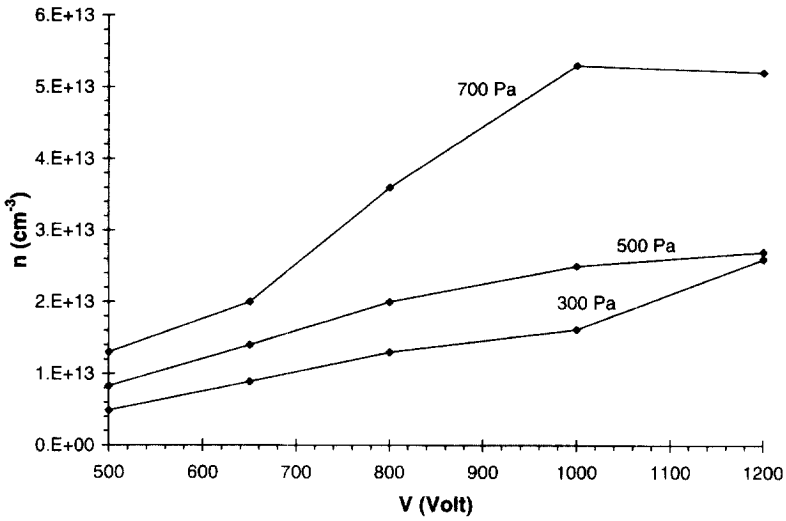

Fig. 16. Calculated densities of the argon 4s $[3/2]_2$ metastable level at the maximum of their profiles, as a function of voltage at three pressures.

800 K and 28 mA. The density is at its maximum at ca. 2 mm from the cathode and decreases further in the discharge. The density at the maximum appears to be somewhat lower than the argon ion density at its maximum (Fig. 5). However, further in the discharge the argon 4s $[3/2]_2$ metastable atom density decreases less rapidly than the argon ion density, so that in general the argon 4s $[3/2]_2$ metastable atom density is somewhat higher than the argon ion density.

The variation of this metastable density (at the maximum of the profile) as a function of voltage and pressure is illustrated in Fig. 16. The density increases with voltage and pressure, but the variation is not so pronounced as for the other plasma species. Indeed, at higher pressure and voltage the populating processes (e.g. excitation from the ground state) become more significant, but at the same time depopulation of the excited levels (e.g. due to excitation to higher levels) gains increasing importance as well, and the net density increase is the result of the

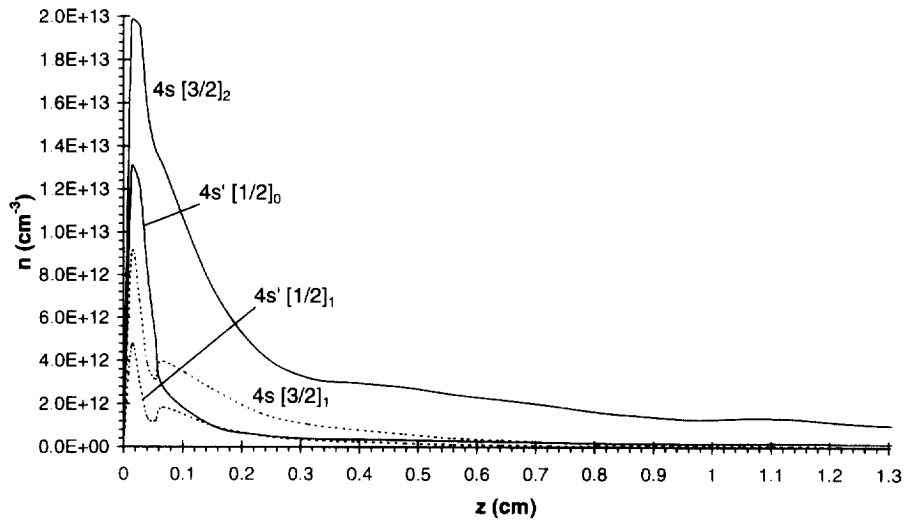

Fig. 17. Calculated one-dimensional density profiles of the four 4s levels at the cell axis at 500 Pa, 800 V and 28 mA (only the first part of the cell is illustrated). Solid lines, metastable levels; dashed lines, non-metastable levels.

competing processes of populating and depopulating the level. Comparing Fig. 6 and Fig. 16 it can be anticipated that at low voltages and pressures the argon 4s $[3/2]_2$ level will play a dominant role in the discharge, whereas at high voltages and pressures the argon ions will come more and more into play (i.e. relative importance of Penning ionization and asymmetric charge transfer for the ionization of sputtered copper atoms, see further).

One-dimensional density profiles of the argon 4s $[3/2]_2$ metastable levels have been measured in a Grimm source with atomic absorption spectrometry by Ferreira et al. [30]. They also found a pronounced maximum adjacent to the cathode, followed by a rapid decrease. Depending on the discharge conditions a second maximum was sometimes observed at about 4 mm from the cathode. A similar second maximum appeared sometimes in our modeling results (see e.g. [8,41]) depending on the discharge conditions and cell geometry. The value of the maximum in the experimental density profiles of [30] was also in the order of 10^{13}cm^{-3} which is in excellent agreement with the results of our calculation. This indicates that our model presents a realistic picture of the behavior of metastable atoms in the discharge.

Besides the 4s $[3/2]_2$ metastable level, argon possesses another 4s metastable level (i.e. the 4s' $[1/2]_0$ level at 11.72 eV) and two 4s non-metastable levels (i.e. the 4s $[3/2]_1$ and 4s' $[1/2]_1$ levels at 11.62 and 11.83 eV, respectively). In Fig. 17 the one-dimensional profiles of these four 4s levels, taken at the cell axis, are depicted. Only the first part of the discharge cell is presented (until $z = 1.3$ cm) because the density profiles decrease further in the cell and they do not provide additional information. It can be seen that the 4s $[3/2]_2$ metastable level has the highest population density, followed by the 4s' $[1/2]_0$ metastable level. The latter is a factor of 1.5 lower at the maximum of the profiles. Further in the discharge cell the ratio of 4s $[3/2]_2$ to 4s' $[1/2]_0$ population densities increases to 5–6 at $z = 0.1$ cm, ca. 7 at $z = 0.2$ cm and in the order of 10 at $z = 0.5$ cm. The ratio of statistical weights for both levels is 5 (i.e. $g = 5$ and 1 for the 4s $[3/2]_2$ and the 4s' $[1/2]_0$ levels, respectively), which therefore correlates reasonably well with the calculated density ratios.

The 4s $[3/2]_1$ and 4s' $[1/2]_1$ levels are somewhat lower in density, because they can decay to the ground state by emission of radiation and are therefore not metastable. However, their density is still rather high, because the emitted radiation is often 'trapped' due to reabsorption by the ground state argon atoms leading again to populating these 4s non-metastable levels. The net escape probability of radiation is in general only in the order of 10^{-3}–10^{-4}, as was demonstrated in [9]. Beside the first maximum close to the cathode the 4s non-metastable levels exhibit a second maximum at about 0.06–0.08 cm from the cathode (i.e. in the beginning of the NG). The first maximum is produced by fast argon ion and atom impact excitation, which is only important close to the cathode where the argon ions and atoms reach sufficiently high energies. The second maximum is due to electron impact excitation, which is indeed most significant in the beginning of the NG. All 4s levels show the same behavior as a function of pressure and voltage as the 4s $[3/2]_2$ metastable level (see Fig. 16) and the corresponding figures are therefore not shown here.

The 4p levels are characterized by the same two peaks as the 4s non-metastable levels, but their density was calculated to be 2–3 orders of magnitude lower. Indeed, the 4p levels can decay to the lower 4s levels without much radiation trapping, since the number densities of 4s levels are much lower than the argon ground state level, and they are not able to reabsorb a large fraction of the emitted radiation. For the low 4p levels the first peak (due to fast argon ion and atom impact excitation) is still higher than the second peak (due to electron impact excitation), while for the higher 4p levels both peaks are comparable in magnitude. Indeed, as the excitation energy of the levels increases ion and atom impact excitation become less efficient, whereas electron impact excitation remains important. The higher excited levels (3d, 5s, 5p, etc) do not exhibit a pronounced peak adjacent to the cathode anymore, because ion and atom impact excitation become more and more negligible. These levels are, therefore, characterized by a single peak in the NG.

3.3. Energies of the plasma species

The energy of the plasma species is calculated explicitly in the Monte Carlo models only. Hence, information can only be obtained about the energy of the electrons, of the argon ions, fast argon atoms

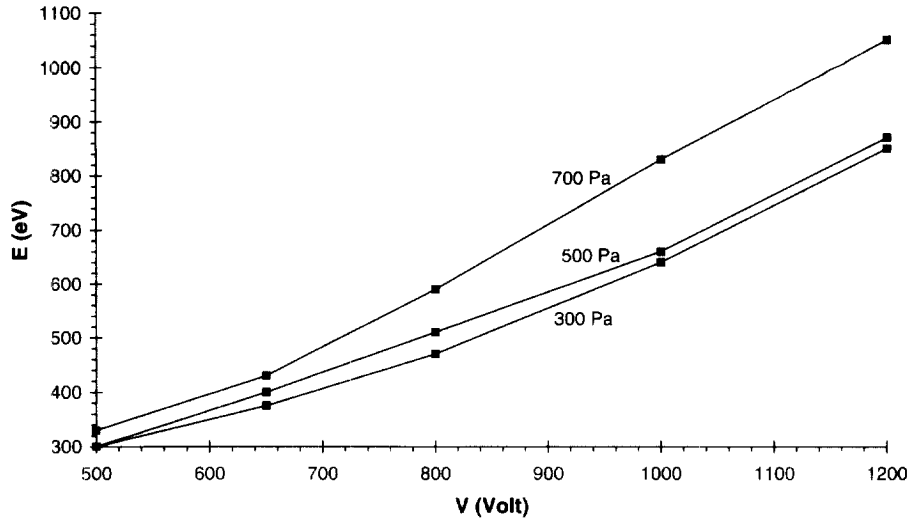

Fig. 18. Calculated maximum mean energies of the fast electrons (i.e. at the end of the CDS), as a function of voltage at three pressures.

and copper ions in the CDS, and of the copper atoms immediately after sputtering from the cathode. The other plasma species, described with the fluid models, are assumed to be thermalized.

The electrons start at the cathode and gain energy in the CDS by the electric field, but they also lose a fraction of this energy by collisions. They reach their maximum energy at the end of the CDS. Indeed, in the NG they will not gain much energy anymore from the weak electric field; they will, however, lose a considerable amount of energy due to collisions. The maximum mean energy of the electrons (i.e. at the end of the CDS) is plotted in Fig. 18 against pressure and voltage. The mean energy increases with rising voltage, as is expected because more energy can be gained from the electric field (higher potential difference). The energy increases also a little bit with pressure. Indeed, although the absolute number of collisions increases with pressure (i.e. there are more gas atoms, hence also more collision targets), the total number of collisions in the CDS seems to decrease because the CDS becomes shorter at higher

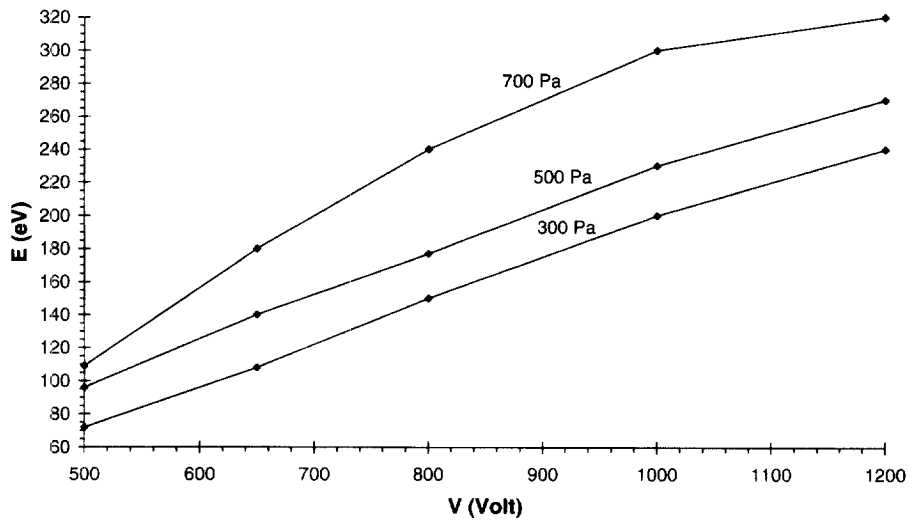

Fig. 19. Calculated maximum mean energies of the argon ions (i.e. at the cathode), as a function of voltage at three pressures.

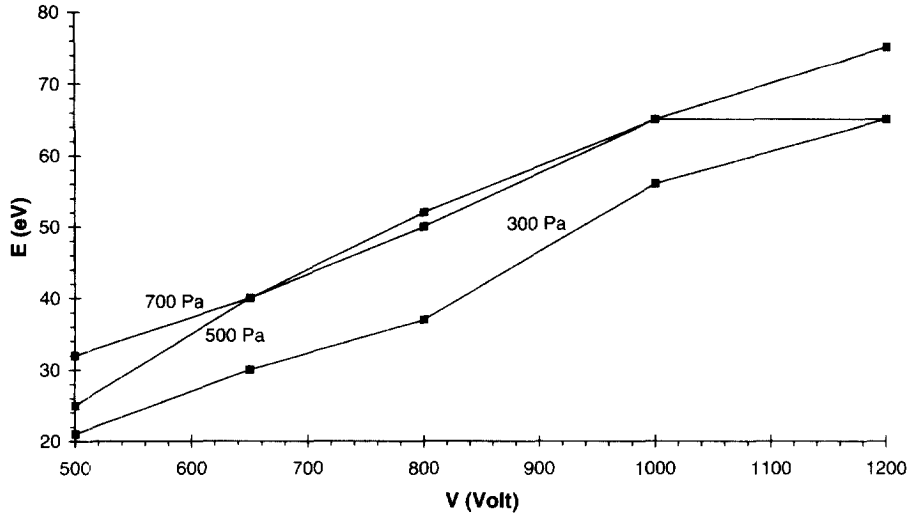

Fig. 20. Calculated maximum mean energies of the fast argon atoms (i.e. at the cathode), as a function of voltage at three pressures.

pressures (see above, Fig. 4). Therefore, the electrons undergo fewer collisions in the CDS, so that they can reach higher energies at the end of the CDS. The maximum mean energy ranges from 300–1000 eV, which corresponds to 60–80% of the operating voltages. These values are somewhat higher than at GDMS conditions (i.e. typically 50% of the discharge voltage [39]), which is attributed to the higher pressures and hence fewer collisions in the CDS (see explanation above). It should be mentioned that Fig. 18 illustrates only the energy of the fast electrons (i.e. the ones able to produce inelastic collisions with argon ground state atoms, with typical energies above ca. 11 eV). The fast electrons, however, constitute only a small part of the total electron population. The largest fraction of electrons (i.e. the slow electrons) are more or less thermalized, so that the overall mean energy of all electrons will probably be around 1 eV.

The argon ions enter the CDS from the NG with more or less thermal energies. They gain also energy from the electric field in the CDS on their way towards the cathode and they reach maximum energies at the cathode. However, the ions lose also energy due to collisions and the energy loss is larger than for the electrons, as appears from Fig. 19 which depicts the maximum mean energy as a function of voltage and pressure. Indeed, the argon ions lose their energy more efficiently due to symmetric charge transfer and scattering elastic collisions. The maximum mean energy increases also with pressure and voltage, for the same reasons as explained above for the electrons. The maximum energy is typically 70–300 eV, which means 15–30% of the discharge voltage. This is again slightly higher than at GDMS conditions where typical values of 10–15% were calculated [39].

Fig. 20 illustrates the effect of pressure and voltage on the maximum mean energies of the fast argon atoms (also at the cathode). These species are created from collisions of the argon ions with energies corresponding to the argon ion energy before collisions. However, being neutral species, they cannot gain additional energy on their way towards the cathode; they can only lose energy due to collisions. Therefore, they reach lower maximum energies at the cathode, i.e. typically 20–70 eV, which corresponds to 4–7% of the operating voltage. For comparison, at GDMS conditions the maximum mean energies at the cathode were calculated to be about 3% of the total voltage [39].

Finally, the maximum mean energies (again at the cathode) of the copper ions are presented in Fig. 21, as a function of pressure and voltage. The copper ions enter the CDS also from the NG with thermal energies and they gain energy from the electric field when traveling to the cathode. As appears from Fig. 21 they do not lose their energy so efficiently due to collisions, because symmetric charge transfer

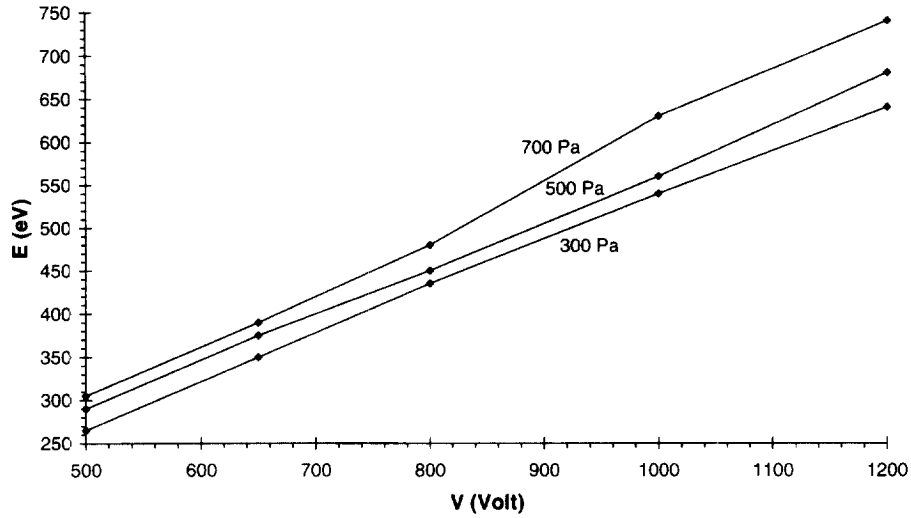

Fig. 21. Calculated maximum mean energies of the copper ions (i.e. at the cathode), as a function of voltage at three pressures.

collisions are not important due to the much lower copper atom density. They reach typically maximum energies of 260–740 eV, which means 50–60% of the total voltage.

3.4. Collision processes in the plasma

Information about collision processes in the plasma can also be obtained from the Monte Carlo models. The various rates of all the collisions incorporated in the models (see above) throughout the complete three-dimensional discharge volume have been calculated. However, showing all these data would lead to a large number of additional figures; therefore, only the most interesting results will be presented here.

3.4.1. Ionization of argon atoms

Argon atoms can be ionized by electron, fast argon ion and atom impact ionization from the ground state, and also by stepwise ionization from excited states

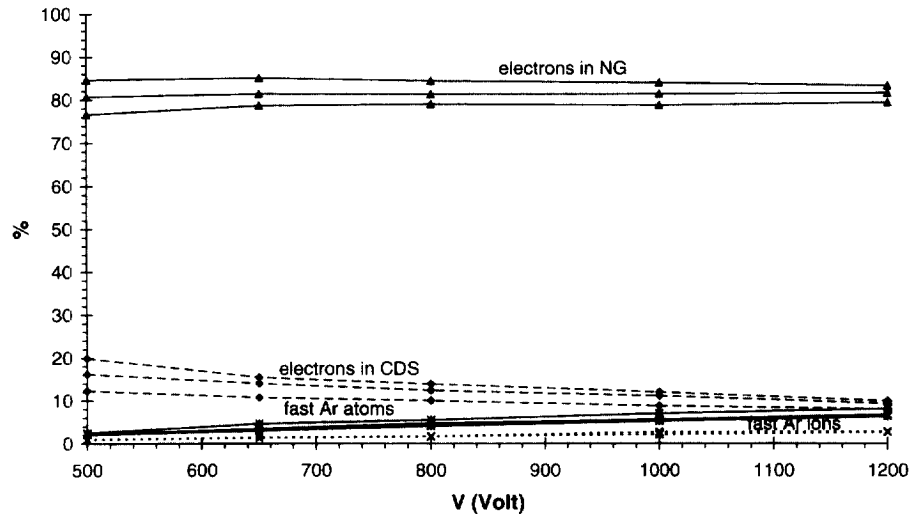

Fig. 22. Calculated relative contributions of electron, fast argon ion and atom impact ionization to the total ionization of argon atoms, integrated over the entire three-dimensional discharge region, as a function of voltage at three pressures.

and by collisions between two argon atoms in the metastable levels. However, the latter two processes are negligible compared to direct ionization from the ground state. Electron impact ionization is most effective around 0.1 cm from the cathode, i.e. in the beginning of the NG where most electrons are present and where they have most suitable energies for ionization. Fast argon ion and atom impact ionization, on the other hand, occur only in the CDS close to the cathode where the ions and atoms reach high enough energies. Fig. 22 shows the relative contributions of electrons, fast argon ions and atoms to the total ionization of argon, integrated over the entire three-dimensional discharge volume. Electron impact ionization in the NG is dominant at all voltages and pressures. It contributes for about 80% and becomes somewhat more significant at increasing pressure due to the shorter CDS and hence longer NG. Electron impact ionization in the CDS is also quite important, with a contribution of about 10% at high pressures (short CDS) to about 20% at lower pressures (longer CDS). It decreases also a little bit at higher voltages, due to the somewhat shorter CDS. Fast argon atom and ion impact ionization play a non-negligible role too: these processes contribute for about 2–8% and 1–3%, respectively, and they become more important at higher voltages, which is logical because the ions and atoms can reach higher energies. The effect of the pressure is almost negligible, as appears from Fig. 22. Therefore the relative contributions calculated for the GD–OES conditions are comparable to the ones obtained for typical GDMS conditions [39].

3.4.2. Ionization of sputtered copper atoms

The sputtered atoms can also be ionized by electron impact ionization. In principle, fast argon ion and atom impact ionization would also be possible, but there are no cross sections available in the literature for copper atoms; hence the latter two processes are not included in the model. In any case, their contribution would be negligible, because two other processes start playing a dominant role for copper atoms, i.e. Penning ionization by argon 4s metastable atoms and asymmetric charge transfer with argon ions. The relative contributions of these three ionization mechanisms are illustrated in Fig. 23 for different voltages and pressures. It appears that electron impact ionization is of minor importance (2–4%) at all discharge conditions investigated and that Penning ionization and asymmetric charge transfer are much more significant. This means that the ionization of copper atoms is much more effective than for argon atoms, for which Penning ionization and asymmetric charge transfer obviously do not come into play; this also explains why the calculated ionization degree of copper is higher than for argon. In general, it can be seen

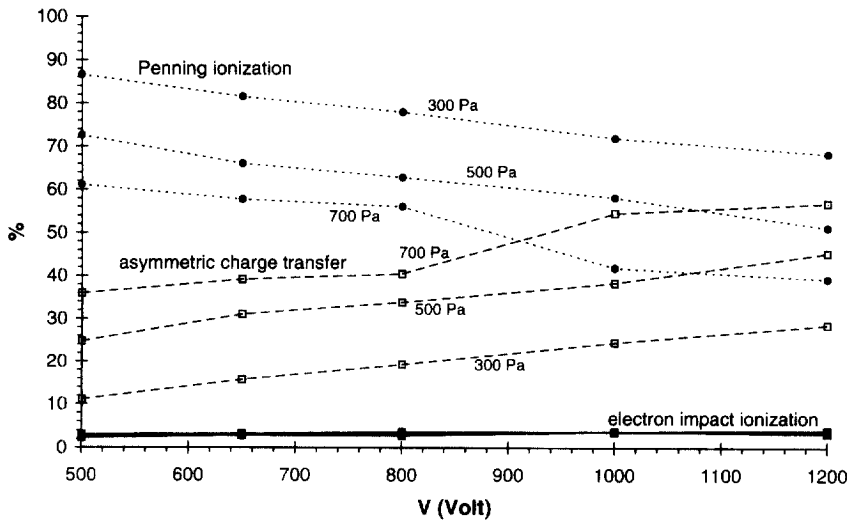

Fig. 23. Calculated relative contributions of Penning ionization, asymmetric charge transfer and electron impact ionization to the total ionization of sputtered copper atoms, integrated over the entire three-dimensional discharge region, as a function of voltage at three pressures.

that Penning ionization is the dominant ionization process for the copper atoms; its contribution ranges from 40–85% and decreases with increasing pressure and also slightly with rising voltage. The variation of the contribution of asymmetric charge transfer with respect to pressure and voltage is exactly opposite; it is only about 10% at low voltages and pressures, and increases to nearly 60% at the highest voltage and pressure investigated. Hence, it appears that in general Penning ionization is the dominant ionization process, but at high voltages and pressures asymmetric charge transfer becomes more important. This trend is consistent with general statements in the literature; at typical GDMS conditions (i.e. rather low pressures) Penning ionization is most significant, whereas asymmetric charge transfer becomes of major importance in glow discharges used for OES, which operate at higher pressures.

In our earlier work we found that asymmetric charge transfer became already dominant at the typical GDMS pressure of 100 Pa [8,39]. The reason for the apparent discrepancy with the present results is that the density of argon metastable atoms is now calculated in a different way (i.e. not only the behavior of this metastable level is considered, but the effect of all other excited levels is explicitly taken

Table 1
Calculated relative contributions (in percent) of various populating and depopulating processes for some excited levels, at 500 Pa, 800 V and 28 mA

Process	$4s[3/2]_2$	$4s[3/2]_1$	$4s'[1/2]_0$	$4s'[1/2]_1$	4p level	3d level	5p level
Populating processes							
Electron impact excitation from ground state	4.3	7.9	1.7	25.9	20.7	35.6	36.7
Fast argon atom impact excitation from ground state	18.2	19.3	53.9	28.2	19.5	1.1	0.75
Fast argon ion impact excitation from ground state	2.6	2.8	7.8	4.1	3.0	0.17	0.10
Electron impact excitation from (lower) 4s levels	–	45.6	5.2	17.0	8.7	1.5	0.15
Electron impact de-excitation from (higher) 4s levels	33.4	2.8	16.0	–	–	–	–
Radiative decay from 4p levels	40.8	21.2	14.9	24.2	–	–	–
Radiative decay from 3d + 5s levels	0.0	0.0	0.0	0.0	38.6	–	–
Radiative decay from 5p levels	0.50	0.31	0.34	0.52	–	7.7	–
Radiative decay from 4d + 6s levels	0.0	0.0	0.0	0.0	2.8	0.0	16.3
Radiative decay from 4f levels	0.0	0.0	0.0	0.0	0.0	7.1	0.0
Radiative decay from higher levels	0.03	0.02	0.01	0.01	1.7	0.95	1.1
Electron impact excitation from lower + de-excitation from higher levels	–	–	–	–	3.1	24.2	23.9
Thermal argon atom impact excitation from lower + de-excitation from higher levels	–	–	–	–	1.6	21.6	20.6
Other	0.17	0.07	0.15	0.07	0.3	0.08	0.4
Loss processes							
Metastable-metastable collisions	20.2	3.7	26.6	2.1	–	–	–
Penning ionization of sputtered copper atoms	14.0	3.5	19.4	2.0	–	–	–
Electron impact excitation to higher 4s levels	58.6	2.4	34.2	–	–	–	–
Electron impact excitation to the 4p levels	6.2	1.1	4.2	0.62	–	–	–
Electron impact ionization	0.47	0.10	0.35	0.06	–	–	–
Two-body and three-body collision with argon atoms	0.39	0.03	0.47	0.03	–	–	–
Electron impact de-excitation to lower 4s levels	–	34.0	14.6	12.6	–	–	–
Radiative decay to the ground state	–	55.0	–	82.3	0.0	0.0	0.0
Radiative decay to the 4s levels	–	–	–	–	99.6	0.0	7.9
Radiative decay to the 4p levels	–	–	–	–	–	78.9	0.0
Radiative decay to the 3d and 5s levels	–	–	–	–	–	–	43.1
Electron impact excitation to higher + de-excitation to lower levels	–	–	–	–	0.26	3.9	22.2
Thermal argon atom impact excitation to higher + de-excitation to lower levels	–	–	–	–	0.11	17.1	26.2
Other	0.14	0.17	0.18	0.29	0.03	0.1	0.6

into account) which apparently yields a higher density, and hence, the relative contribution of Penning ionization is now calculated to be higher than with the previous model. Therefore, direct comparison with our earlier results for GDMS conditions is not possible. It shows also that the exact values of the calculated relative contributions have to be considered with caution, since a somewhat different model yields different values for the contributions and, moreover, the cross sections of Penning ionization and especially of asymmetric charge transfer are subject to uncertainties. However, the general outcome and the dependence on voltage and pressure will be reliable. Nevertheless, it should be mentioned that these results cannot be generalized to all elements, because asymmetric charge transfer is very element-specific (i.e. dependent on the number of suitable energy levels of the element ion [42]). For copper, Steers has indeed demonstrated, based on the intensity of specific emission lines, that asymmetric charge transfer with argon ions occurs in a Grimm source [43].

3.4.3. Populating and depopulating processes for the argon excited levels

As mentioned before, a large number of populating and depopulating processes for the various excited levels are taken into account in the model, i.e. electron, argon ion, fast and thermal argon atom impact ionization from all levels, excitation and de-excitation between all levels, electron–ion three-body recombination where the third body is an electron, argon ion, fast or thermal argon atom, and radiative recombination, to all levels, and finally, radiative decay between all levels. All these processes are described in detail in [9].

Table 1 presents the calculated relative contributions of various populating and depopulating processes at 500 Pa, 800 V and 28 mA, for the four 4s levels, a 4p, a 3d and a 5p level. The 4p and 5p levels are of great interest, because they give rise to the most intense spectral lines in the argon spectrum, i.e. the so-called 'red' and 'blue' lines, respectively.

It appears from Table 1 that the four 4s levels are primarily populated by fast argon atom, ion and electron impact excitation from the ground state, and also by electron impact excitation from the lower or de-excitation from the higher 4s levels. Moreover, radiative decay from the 4p levels is very important. For the 4p levels, fast argon ion and atom impact excitation from the ground state are still significant, but these processes become of minor importance for the higher levels (3d, 5s, 5p and higher), because the energies of these levels become too high for efficient excitation. Electron impact excitation from the ground state, and also (to a less extent) from the 4s levels, remains important. Radiative decay from higher levels remains quite significant too. Moreover, electron and thermal argon atom impact excitation from nearby lower levels and de-excitation from nearby higher levels come into play for the 3d and 5p levels, and these processes will even gain importance for higher excited levels, as the energy spacing between levels becomes smaller [9].

As far as the loss processes are concerned the two 4s metastable levels are primarily depopulated by collisions between two atoms in metastable levels, Penning ionization of sputtered atoms and electron impact excitation to the higher 4s or de-excitation to the lower 4s levels. Also electron impact excitation to the 4p levels contributes for a few percent. The above processes also play a minor role in the depopulation of the two non-metastable 4s levels, although the majority of loss is attributed to radiative decay (in spite of the large fraction of radiation trapping). For the higher excited levels (4p, 3d, 5p) radiative decay to lower levels is by far the dominant depopulating process, although for the 5p and higher levels, electron and thermal argon atom impact excitation to nearby higher and de-excitation to nearby lower levels become increasingly important.

We have also investigated the effect of pressure and voltage on the relative contributions of the various (de)populating processes. It appeared that at increasing pressure, electron impact excitation and de-excitation between the 4s levels are gaining importance, both for populating and depopulating the levels, as well as electron and thermal argon atom impact excitation and de-excitation within higher excited levels. On the other hand, electron, argon ion and fast atom impact excitation from the ground state, and radiative decay, become less significant, as well as metastable–metastable collisions and Penning ionization of sputtered atoms for the metastable levels. The effect of voltage was found to be less

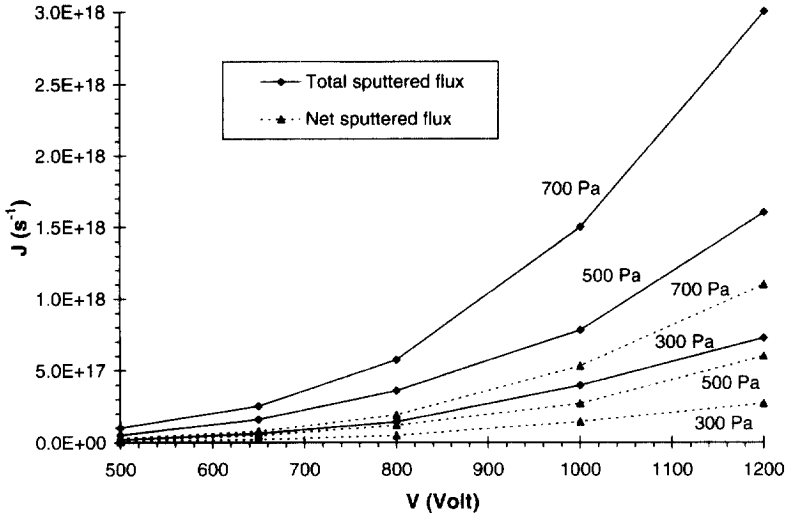

Fig. 24. Calculated fluxes of sputtered copper atoms at the cathode, as a function of voltage at three pressures. Solid lines, total flux of sputtered atoms; dashed lines, net flux of sputtered atoms.

pronounced. Fast argon ion and atom impact excitation from the ground state play a somewhat more important role at increasing voltages, at the expense of electron impact excitation. Moreover, Penning ionization gains importance as a loss process for the metastable levels, due to the higher sputtered atom densities at increasing pressure. The relative contributions of the other populating and depopulating processes remained more or less independent of voltage changes.

3.4.4. Sputtering and resulting crater profiles at the cathode

A last outcome from the models which will be dealt with here, and which is very important from the analytical point of view, is sputtering at the cathode. Fig. 24 illustrates the effect of pressure and voltage on the flux of sputtered copper atoms from the cathode. The sputtered flux increases with pressure and voltage, as is expected. Indeed, higher voltages and pressures yield higher currents and this results in

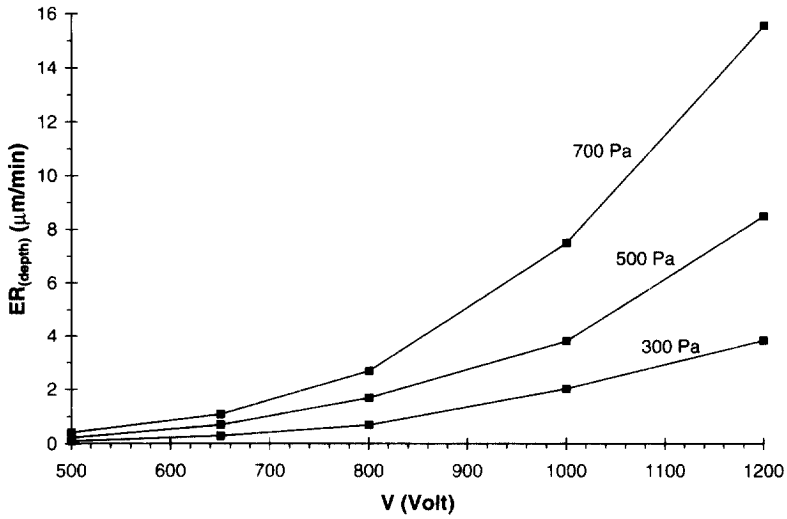

Fig. 25. Calculated erosion rates (in depth per time unit), as a function of voltage at three pressures.

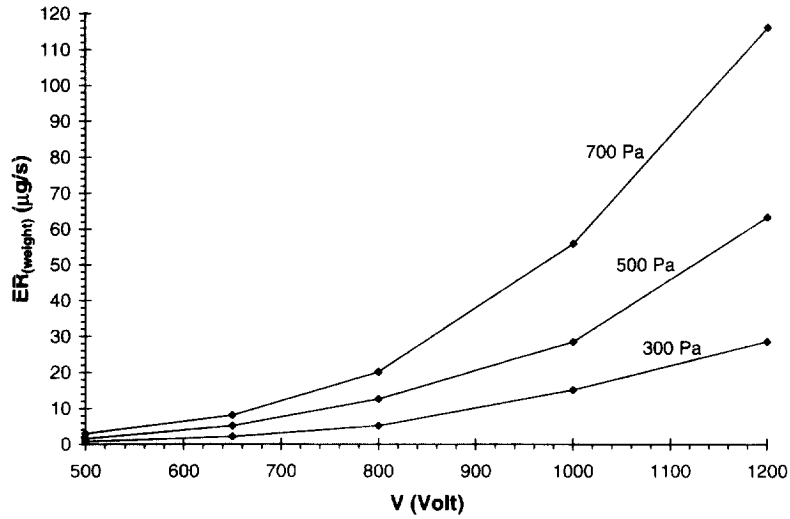

Fig. 26. Calculated erosion rates (in weight per time unit), as a function of voltage at three pressures.

more sputtering from the cathode. Moreover, at increasing voltages the bombarding species can reach higher energies, which makes the sputtering process more efficient. A fraction of the sputtered atoms will diffuse back towards the cathode where they will be redeposited. The difference between the total sputtered flux and the backdiffusion flux yields the net flux of sputtered atoms, which also increases with pressure and voltage, as follows from Fig. 24. In general, the net sputtered flux amounts about 30–40% of the total sputtered flux; or in other words about 60–70% of the originally sputtered atoms are again redeposited onto the cathode. This number is somewhat higher than the typical values calculated for GDMS conditions (i.e. 40–65%).

It is the net flux of sputtered atoms (i.e. total sputtered flux minus backdiffusion flux) which gives rise to erosion of the cathode. The erosion rates are computed from the calculated net flux of sputtered atoms by:

$$ER_{(\text{depth})} = j_{\text{sput,net}} \frac{M}{N_A \rho} \quad ER_{(\text{weight})} = J_{\text{sput,net}} \frac{M}{N_A}$$

where $ER_{(\text{depth})}$ and $ER_{(\text{weight})}$ are the erosion rates in depth per unit time (cm s^{-1}) and in weight per unit time (g s^{-1}), respectively. $J_{\text{sput,net}}$ and $j_{\text{sput,net}}$ are the calculated net flux and flux density of sputtered atoms, expressed in s^{-1} and in $cm^{-2}s^{-1}$, respectively. M is the atomic weight (g mol^{-1}), N_A is Avogadro's number and ρ is the density of the sample material (ρ_{Cu} = 8.92 g cm^{-3} [44]). The resulting erosion rates are plotted for a range of pressures and voltages in Figs 25 and 26. The erosion rate in depth per unit time was calculated to vary from 0.1 to 15 μm min^{-1} for the discharge conditions under study (with most values lying between 0.1 and 5 μm min^{-1}), whereas the computed erosion rate in weight per unit time increased from 0.7 μg s^{-1} at low voltages and pressures to about 115 μg s^{-1} at the highest voltage and pressure investigated (with the majority of values between 0.7 and 30 μg s^{-1}). These calculated values are in reasonable agreement with data found in the GD–OES literature. Indeed, Bengtson et al. reported typical values of 10–100 nm s^{-1}, which corresponds to 0.6–6 μm min^{-1} [45]. In [46] experimental sputtering rates at 800 V and 50 mA were tabulated for a variety of cathode materials and the values ranged from 0.8 to 6 μm min^{-1}. Copper was not included in this table, but our calculated value for 800 V and 700 Pa (which yields a current of 45 mA) is found to be 2.7 μm min^{-1}, which lies perfectly in the range of tabulated values. We calculated also the erosion rates with Boumans' classical formula for sputtering [47]:

$$ER_{(\text{weight})} = C_q I(V - V_0)$$

where C_q and V_0 are constants depending on the cathode material and the gas, but independent of

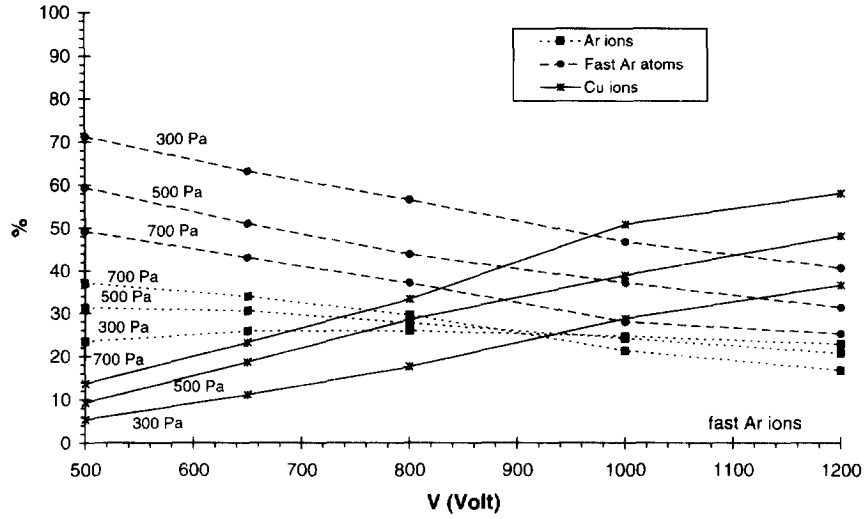

Fig. 27. Calculated relative contributions of fast argon atoms, argon ions and copper ions to the sputtering at the cathode, as a function of voltage at three pressures.

pressure, current and voltage (C_q = 0.84 μg (W s)$^{-1}$ and V_O = 360 V). For the voltages and currents under study here we obtained values with this formula ranging from 0.4–80 μg s^{-1}, which correspond reasonably well with our modeling results (the latter are only a factor of two higher, which is not too bad in view of the fact that our model is completely self-consistent and uses only pressure, voltage and gas temperature as input values).

Fig. 27 presents the relative contributions of fast argon atoms, argon ions and copper ions to the sputtering process. At low voltages and pressures, the fast argon atoms play a dominant role in sputtering (e.g. ca. 70% at 500 V and 300 Pa, compared to about 25% and 5% for the argon ions and copper ions, respectively). However, when pressure and voltage increase the contribution of fast argon atoms decreases significantly. At the same time the copper ions gain increasing importance for sputtering and they even become dominant at the highest pressure and voltage investigated (i.e. 700 Pa, 1200 V) with a contribution of about 60%, whereas the fast argon atoms and ions each contribute for about 20%. The reason for this is straightforward. At high pressures and voltages there is a large amount of sputtering and a lot of copper ions are being formed. As follows from Fig. 6 and Fig. 13 the density of copper ions has become comparable to the argon ion density and the same is true for the fluxes of both ion species. Moreover, the mean energy of copper ions bombarding the cathode is clearly higher than the mean energy of argon ions, as appears from the comparison of Fig. 19 and Fig. 21. Hence, since the efficiency of sputtering increases with the energy of the bombarding species, it is indeed to be expected that the role of copper ions to the sputtering process (called 'self-sputtering') becomes so important. At typical GDMS conditions we found that self-sputtering played only a minor role (a few %), whereas the largest amount of sputtering was due to fast argon atoms (contribution of about 70%) and the argon ions contributed for about 25–30%. Hence, the role of copper ions has increased significantly at GD–OES compared to GDMS conditions.

Finally, the model is able to calculate the net sputtering (or erosion) rate on the cathode as a function of radial position, which gives rise to the crater profile. To obtain good depth resolution in depth profiling analysis, flat crater bottoms are desirable. In previous work, at typical GDMS conditions and for the standard cell of analysing flat samples in the VG9000 glow discharge mass spectrometer, we have calculated crater profiles with a pronounced crater edge effect, i.e. the calculated craters were much deeper at the edges than in the center [12]. This was also found back in experimental crater profiles measured

with the VG9000 mass spectrometer [48]. At the GD–OES conditions under study here this crater edge effect is not observed in the calculation results. Indeed, the crater bottoms computed here are rather flat or even somewhat concave (i.e. slightly deeper in the center than at the edges). The latter is in good accordance with [12,48] where it was found that the crater bottom changes from convex to flat and concave at increasing pressure. The present results also suggest that the Grimm source at GD–OES conditions is probably more suitable for depth profiling than the VG9000 glow discharge cell at GDMS conditions, which may explain why the first cell is more commonly used for depth profiling than the latter one.

4. Conclusion

A comprehensive set of models for a direct current glow discharge in argon, which has been developed previously for typical GDMS conditions, has been applied in the present work to a Grimm source used for GD–OES. Typical calculation results (e.g. the electrical current as a function of voltage and pressure, the potential distribution, the lengths of the CDS, the densities and energies of the plasma species, information about the collision processes in the plasma and about sputtering at the cathode) have been shown and discussed for typical GD–OES conditions. Moreover, the results have been compared with values calculated for GDMS conditions. The effect of pressure and voltage on the calculation results has been investigated. Generally, when pressure and voltage increase the current rises also, as well as the densities and fluxes of the various plasma species. Moreover, the ionization degrees of argon atoms and of sputtered copper atoms become higher, and the copper atoms and ions gain increasing importance in the discharge. The latter effect is most clearly manifested in the contribution of copper ions to the sputtering process, i.e. self-sputtering, which even becomes dominant at the highest pressure and voltage investigated.

In future work we plan to use the present model (more specifically the submodel describing the behavior of the argon excited levels) in combination with a collisional-radiative model for the copper excited levels (which has still to be developed) to calculate the optical emission spectrum of argon and copper, and to investigate the effect of pressure, voltage and current on some characteristic emission lines, because this is of direct analytical importance for GD–OES.

Acknowledgements

A. Bogaerts is indebted to the Flemish Fund for Scientific Research (FWO-Flanders) for financial support. The authors also acknowledge financial support from the Federal Services for Scientific, Technical and Cultural Affairs (DWTC/SSTC) of the Prime Minister's Office through IUAP-IV (Conv. P4/10).

References

[1] A. Bogaerts, M. Straaten, R. Gijbels, Spectrochim. Acta Part B 50 (1995) 179.
[2] A. Bogaerts, R. Gijbels, W.J. Goedheer, J. Appl. Phys. 78 (1995) 2233.
[3] A. Bogaerts, R. Gijbels, W.J. Goedheer, Anal. Chem. 68 (1996) 2296.
[4] A. Bogaerts, R. Gijbels, J. Appl. Phys. 78 (1995) 6427.
[5] A. Bogaerts, R. Gijbels, Phys. Rev. A52 (1995) 3743.
[6] A. Bogaerts, M. Straaten, R. Gijbels, J. Appl. Phys. 77 (1995) 1868.
[7] A. Bogaerts, R. Gijbels, J. Appl. Phys. 79 (1996) 1279.
[8] A. Bogaerts, R. Gijbels, Anal. Chem. 68 (1996) 2676.
[9] A. Bogaerts, R. Gijbels, J. Vlcek, J. Appl. Phys. (submitted).
[10] A. Bogaerts, R. Gijbels, Fres. J. Anal. Chem. 355 (1996) 853.
[11] A. Bogaerts, R. Gijbels, Spectrochim. Acta Part B 52 (1997) 553.
[12] A. Bogaerts, R. Gijbels, Spectrochim. Acta Part B 52 (1997) 765.
[13] A. Bogaerts, R. Gijbels, J. Anal. Atom. Spectrom. 12 (1997) 751.
[14] A. Bogaerts, R. Gijbels, J. Am. Soc. Mass Spectrom. 8 (1997) 1021.
[15] W. Grimm, Spectrochim. Acta Part B 23 (1968) 443.
[16] J.A.C. Broekaert, K.R. Brushwyler, C.A. Monnig, G.M. Hieftje, Spectrochim. Acta Part B 45 (1990) 769.
[17] Z. Weiss, Spectrochim. Acta Part B 47 (1992) 859.
[18] R. Payling, D.G. Jones, S.A. Gower, Surf. Int. Anal. 20 (1993) 959.
[19] K. Florian, W. Fischer, H. Nickel, J. Anal. Atom. Spectrom. 9 (1994) 257.
[20] A. Bengtson, Spectrochim. Acta Part B 49 (1994) 411.
[21] V. Hoffmann, G. Ehrlich, Spectrochim. Acta Part B 50 (1995) 607.
[22] Z. Weiss, J. Anal. Atom. Spectrom. 12 (1997) 159.
[23] E.B.M. Steers, F. Leis, J. Anal. Atom. Spectrom. 12 (1997) 307.

[24] N. Jakubowski, D. Stuewer, G. Toelg, Int. J. Mass Spectrom. Ion Proc. 71 (1986) 183.
[25] N. Jakubowski, D. Stuewer, W. Vieth, Anal. Chem. 59 (1987) 1825.
[26] N. Jakubowski, D. Stuewer, J. Anal. Atom. Spectrom. 7 (1992) 951.
[27] N. Jakubowski, I. Feldmann, D. Stuewer, J. Anal. Atom. Spectrom. 12 (1997) 151.
[28] N.P. Ferreira, H.G.C. Human, L.R.P. Butler, Spectrochim. Acta Part B 35 (1980) 287.
[29] N.P. Ferreira, H.G.C. Human, Spectrochim. Acta Part B 36 (1981) 215.
[30] N.P. Ferreira, J.A. Strauss, H.G.C. Human, Spectrochim. Acta Part B 37 (1982) 273.
[31] E.B.M. Steers, F. Leis, Spectrochim. Acta Part B 46 (1991) 527.
[32] N.I. Uzelac, F. Leis, Spectrochim. Acta Part B 47 (1992) 877.
[33] M. Kuraica, N. Konjevic, M. Platisa, D. Pantelic, Spectrochim. Acta Part B 47 (1992) 1173.
[34] K. Wagatsuma, K. Hirokawa, Spectrochim. Acta Part B 48 (1993) 1039.
[35] A. Bogaerts, A. Quentmeier, N. Jakubowski, R. Gijbels, Spectrochim. Acta Part B 50 (1995) 1337.
[36] I.R. Videnovic, N. Konjevic, M.M. Kuraica, Spectrochim. Acta Part B 51 (1996) 1707.
[37] M.M. Kuraica, N. Konjevic, I.R. Videnovic, Spectrochim. Acta Part B 52 (1997) 745.
[38] K. Tsuji, H. Matsuta, K. Wagatsuma, Jpn J. Appl. Phys. 36 (1997) L446.
[39] A. Bogaerts, Ph.D. Thesis, University of Antwerp, Antwerp, 1996.
[40] A. Bogaerts, E. Wagner, B.W. Smith, J.D. Winefordner, D. Pollmann, W.W. Harrison, R. Gijbels, Spectrochim. Acta Part B 52 (1997) 205.
[41] A. Bogaerts, R.D. Guenard, B.W. Smith, J.D. Winefordner, W.W. Harrison, R. Gijbels, Spectrochim. Acta Part B 52 (1997) 219.
[42] A. Bogaerts, R. Gijbels, J. Anal. Atom. Spectrom. 11 (1996) 841.
[43] E.B.M. Steers, R.J. Fielding, J. Anal. Atom. Spectrom. 2 (1987) 239.
[44] R.C. Weast, M.J. Astle, CRC Handbook of Chemistry and Physics, 63rd edn, CRC, Boca Raton, 1982–1983.
[45] A. Bengtson, M. Lundholm, J. Anal. Atom. Spectrom. 3 (1988) 879.
[46] H. Hocquaux, Thin film analysis, in: R. K. Marcus (Ed.), Glow Discharge Spectroscopies, Plenum, New York, 1993, p. 346.
[47] P.W.J.M. Boumans, Anal. Chem. 44 (1972) 1219.
[48] C. Jonkers, Ph.D. Dissertation, University of Antwerp, 1995.